Proceedings of Meetings on Acoustics

Exploring the Feasibility of a Thermoacoustic Metastructure for Energy Harvesting and Noise Mitigation

--Manuscript Draft--

Manuscript Number:	POMA-D-22-00147R1
Full Title:	Exploring the Feasibility of a Thermoacoustic Metastructure for Energy Harvesting and Noise Mitigation
Article Type:	ASA Meeting Paper
Corresponding Author:	James Manimala Oklahoma State University College of Engineering Architecture and Technology Stillwater, OK UNITED STATES
Order of Authors:	Samarjith Biswas
	James Manimala
Abstract:	The thermoacoustic effect provides a means to convert acoustic energy to heat and vice versa without the need for moving parts. This could enable the realization of mechanically-robust, noise mitigating energy harvesters via the development of thermoacoustic metastructures using additive and hybrid fabrication processes and materials. The mechanical, thermal and geometric properties of the porous stack that forms a set of acoustic waveguides in thermoacoustic metastructures are key to their performance. In this proof-of-concept study, firstly, various ceramic and polymeric stack designs are evaluated using a custom-built thermoacoustic test rig. Influence of stack parameters such as material, length, location, porosity and pore geometry are correlated to simulations using DeltaEC, a software tool based on Rott's linear approximation. Preliminary results also show a reduction in sound pressure level of around 5.28 dB across the thermoacoustic metastructure at resonance (117.5 Hz). An acousto-thermo-electric transduction scheme is employed to harvest useable electrical power using the best performing stack. Steady-state peak voltage generated was 33 mV for a temperature difference of about 30 degree Celsius across the stack at resonance. Further investigations are underway to establish structure-performance relationships by extracting scaling laws for power-to-volume ratio and frequency-thermal gradient dependencies.
Section/Category:	Engineering Acoustics
Additional Information:	
Question	**Response**
Please provide the JASA Scitation DOI link to the published Meeting Abstract. (Published Abstracts can be accessed through the Journal of the Acoustical Society of America (JASA's) Scitation pg.- https://asa.scitation.org/journal/jas). Search by original title using the magnifier at the top right. An example DOI is - https://doi.org/10.1121/1.4805331. (Please copy and paste your DOI into the space provided.)	https://doi.org/10.1121/10.0011025
Provide the JASA Volume, Issue, and Year info. associated with this DOI link, e.g., Vol. 144, (3) (2018).	151, A179 (2022)

Proceedings of Meetings on Acoustics

Volume 46 http://acousticalsociety.org/

182nd Meeting of the Acoustical Society of America

Denver, Colorado

23-27 May 2022

*Engineering Acoustics: Paper 3pEA3

Exploring the Feasibility of a Thermoacoustic Metastructure for Energy Harvesting and Noise Mitigation

Samarjith Biswas and James Manimala

Mechanical and Aerospace Engineering, Oklahoma State University College of Engineering Architecture and Technology, Stillwater, OK, 74078; samarjith.biswas@okstate.edu; james.manimala@okstate.edu

The thermoacoustic effect provides a means to convert acoustic energy to heat and vice versa without the need for moving parts. This could enable the realization of mechanically-robust, noise mitigating energy harvesters via the development of thermoacoustic metastructures using additive and hybrid fabrication processes and materials. The mechanical, thermal and geometric properties of the porous stack that forms a set of acoustic waveguides in thermoacoustic metastructures are key to their performance. In this proof-of-concept study, firstly, various ceramic and polymeric stack designs are evaluated using a custom-built thermoacoustic test rig. Influence of stack parameters such as material, length, location, porosity and pore geometry are correlated to simulations using DeltaEC, a software tool based on Rott's linear approximation. Preliminary results also show a reduction in sound pressure level of around 5.28 dB across the thermoacoustic metastructure at resonance (117.5 Hz). An acousto-thermo-electric transduction scheme is employed to harvest useable electrical power using the best performing stack. Steady-state peak voltage generated was 33 mV for a temperature difference of about 30 degree Celsius across the stack at resonance. Further investigations are underway to establish structure-performance relationships by extracting scaling laws for power-to-volume ratio and frequency-thermal gradient dependencies.

ASA Best Student Paper Award for Student Presenters

1. INTRODUCTION

The thermoacoustic phenomenon is manifested due to instability caused by acoustic pressure waves propagating in a waveguide containing a fluid medium inducing oscillations in a porous stack, the ends of which are held under an imposed thermal gradient, thereby creating fluctuations in the rate of heat transfer. This, in turn, generates further pressure oscillations, leading to an unstable acoustic mode that can be harnessed without the need for any moving parts. Tracing their origins in early investigations by Rijke [1], Helmholtz [2], and Kirchhoff [3] studies to understand and apply thermoacoustics have been significantly expanded in recent times through the contributions of Rott [4–6], Swift [7–9] and Tijani [10] among others. Thermoacoustic devices, which are broadly classified as heat engines or refrigerators, offer the advantage of having little to no moving parts and relatively quiet operation [11–14]. They can be operated in standing or traveling wave modes. They have been used as an alternative to conventional prime movers to drive cryocoolers [15]. Thermoacoustic refrigerators have also been explored for sustainable cooling applications [16]. Traditionally, practical implementations of thermoacoustic devices have had challenges related to low efficiency [14, 17] and the low power-to-volume ratio [18]. With current additive and hybrid fabrication processes and materials reaching commercial maturity, opportunities exist to utilize them to realize more affordable, lightweight, compact, and efficient components such as the stack for the next generation of thermoacoustic devices.

For the one-dimensional case, the thermoacoustic phenomenon in the linear regime is governed by Rott's approximation [5] which can be simulated using the open-source software, DeltaEC [19]. A typical thermoacoustic refrigerator (TAR) consists of an acoustic waveguide or resonator equipped with an acoustic driver at one end and housing a porous structure called the stack across which the temperature gradient is established using hot (source-side) and cold-side heat exchangers. For the heat engine configuration, heat input is provided using the heat exchangers to generate acoustic waves that drive a prime mover in place of the acoustic driver. In addition to the design of the waveguide and selection of the working fluid, the stack plays a crucial role in the working of a TAR. The material properties and the geometric design of the stack in relation to the properties of the working fluid have key implications for the efficiency of the device.

There are four major approaches to harnessing energy from the acoustical pressure waves-Electromagnetic devices, piezoelectric transducers, Magnetohydrodynamic generators, and bidirectional turbines [20]. Piezoelectric and electromagnetic materials are the most popular approaches to harnessing energy from acoustic or thermoacoustic sources [21]. Piezoelectric materials can generate electricity due to mechanical deformation caused by incident sound waves [22-23]. Piezoelectric harvesters are more feasible and efficient for acoustic excitations at higher frequencies and sound pressure levels [24-26].

The energy conversion efficiency of most conventional harvesters is influenced by the electromechanical coupling factor. Noh *et al.* [27] have reported 0.1 μW power generation using a piezoelectric (PVDF) cantilever beam placed inside a Helmholtz resonator. Khan *et al*. [28] used a Helmholtz resonator and a permanent magnet along with a flexible membrane and generated power of 789.65 μW power from an acoustic source at 100 dB. Khan and Izhar [29] integrated both piezoelectric and electromagnetic approaches and were able to harvest 49 μW from the piezoelectric transducer and 3.16 μW from the electromagnetic transducer from a 130 dB sound source. These studies indicate that usable electric power can be harvested through electromagnetic and piezoelectric transduction of acoustic energy. However, such harvesters typically require multiple, precisely-tuned, static, and moving sub-components [20] that are more susceptible to wear and tear.

In this study, drawing inspiration from acoustic metamaterials, a Thermoacoustic Metastructure (TAMS) that uses an acousto-thermo-electric transduction scheme is developed and evaluated. At the core of TAMS is the stack, a porous structure with tuned geometric and thermophysical properties. The energy transduction process is accomplished through a combination of a thermoacoustic refrigerator coupled to a thermoelectric generator. Firstly, various additively-manufactured TAMS stacks are evaluated against more conventional ceramic stacks using experiments to gauge the influence of material and geometric parameters on their performance. Next, the best performing TAMS is evaluated for energy harvesting. The feasibility of utilizing the versatility provided by additive and hybrid fabrication processes to develop innovative stack geometries that could enable practical solutions for more efficient thermoacoustic devices, especially for multifunctional applications is demonstrated.

2. CONCEPT

Due to the lack of moving parts, operational simplicity, and mechanical robustness, the thermoacoustic transduction approach provides an attractive energy harvesting solution with low maintenance [30]. This makes them a good candidate for applications in remote or harsh environments [31-32]. Predominantly, thermoacoustic energy harvesters that utilize available waste heat to create acoustic waves that are then harnessed to create electric power using different approaches have been widely studied [33-34]. On the other hand, the use of thermoacoustics to harvest usable power from ambient acoustic energy is much less explored, primarily due to the lower available energy densities for practical sources. However, this approach could conceivably also present opportunities for acoustic noise mitigation, and sensing and monitoring functionalities when embedded into infrastructural building-blocks. A thermoacoustic metastructure design that has a high power-to-volume ratio and is rugged, easy to fabricate, and cost-effective would be desirable. A conceptual schematic depicting the implementation envisioned for a TAMS infrastructural barrier is shown in Figure 1. The TAMS infrastructural barrier consists of an acoustic resonator with a thermoacoustic stack embedded within modular infrastructural building-blocks that could be arrayed as a barrier separating a noise-rich urban environment from residential communities that can benefit from acoustic shielding. The resonator and stack would be tuned to the dominant spectral content of the noise so as to maximize harvested energy. Bulk absorbers such as foams or porous materials could also be used in conjunction with TAMS in these building-blocks to address broadband high-frequency noise. In-situ rechargeable batteries can be used to store the harvested energy which could power sensing and monitoring electronics. Further, the analysis of the harvesting signal could yield diagnostic data regarding the field environment via its acoustic signature. Thus, TAMS could provide a rugged, multifunctional solution in several application scenarios.

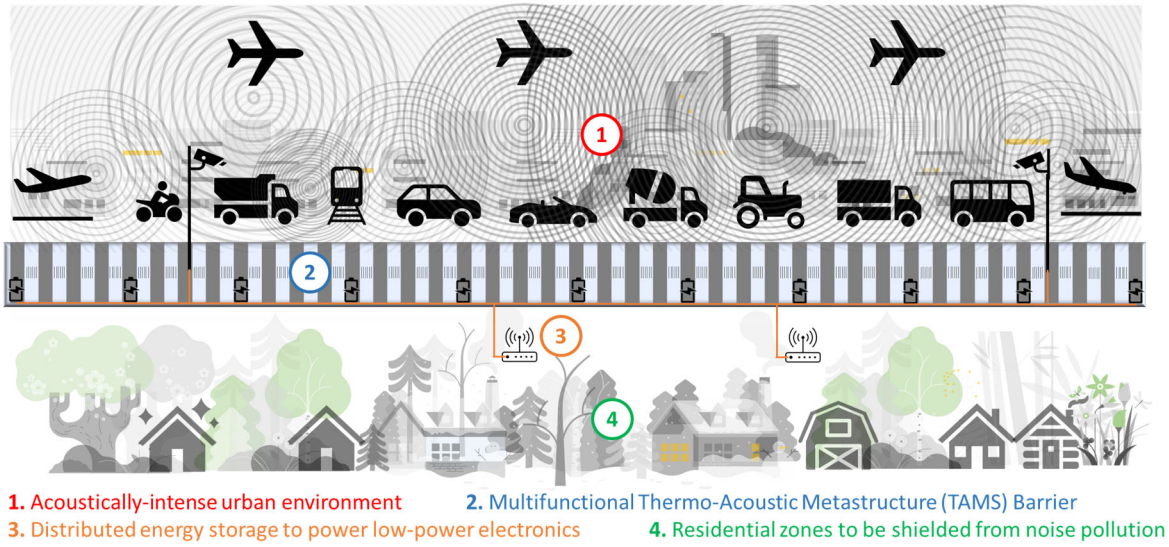

Figure 1. Conceptual depiction of a TAMS infrastructural barrier

3. MATERIALS AND METHODS

The complete experimental setup to evaluate TAMS designs consists of two parts: a thermoacoustic refrigerator (TAR) unit and a thermoelectric generator (TEG) unit. An experimental parametric study is conducted on ceramic and additively manufactured (AM) stack designs using the TAR. Details of the experimental setup, design, and fabrication of the test stacks and the test cases investigated are presented.

A. EXPERIMENTAL SETUP

A benchtop thermoacoustic test rig shown in Figure 2 was constructed to evaluate the stacks. The test rig consists of an acrylic tube waveguide equipped with an acoustic driver (speaker) at one end and capped using a hard rubber end-stop at the other end. The waveguide has a length of 1.524 m and a diameter of 0.101 m. The test stack can be positioned at a specific location along the axis of the tube. A function generator coupled with a signal conditioner and amplifier is used to provide the input excitation for the 50 W speaker. K-type digital

thermocouples with a resolution of 0.1 °C placed at the source and receiver sides of the stack are used to measure the hot and cold-side temperatures, respectively. Microphones with a resolution of 0.1 dB are used to verify the source and receiver-side sound pressure levels. A DAQ computer is used to record all data. The acoustic excitation is applied at discrete frequencies within the frequency range of interest that spans the fundamental resonance frequency of the tube. For all tests, the sound pressure level was maintained at about 138 dB as measured under steady-state conditions within the tube. The entire tube assembly is wrapped in insulating foam during testing to minimize thermal and acoustic flanking paths.

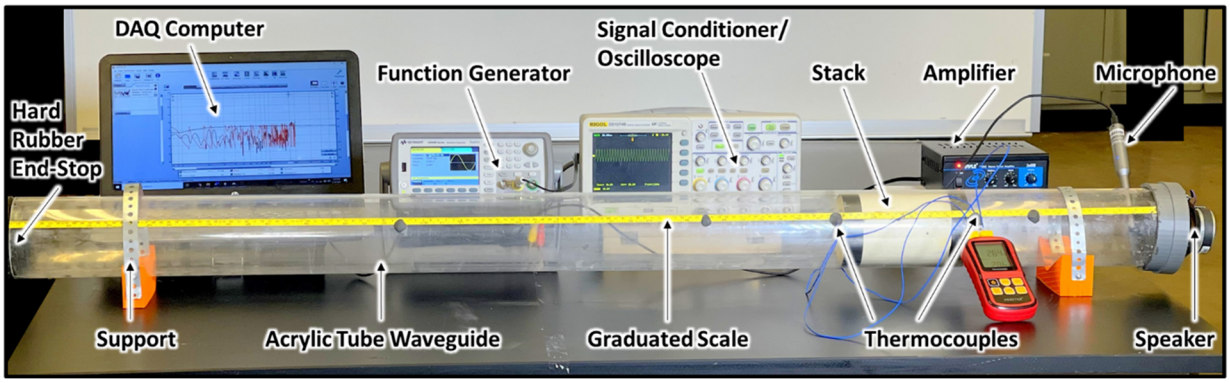

Figure 2. Thermoacoustic refrigerator test rig.

A schematic depiction of the TAR unit of the test rig denoting the experimental parameters is shown in Figure 3. Air under ambient conditions ($P_m = 1\ atm, T_m = 21$ °C) is used as the working fluid in this case. The fundamental resonant frequency of a standing wave tube with a closed end can be computed using the relation,

$$f_o = \frac{c}{2L_s'} \tag{1}$$

Accounting for the effective length of the tube L_s', this gives a theoretical fundamental resonance frequency of 114.5 Hz under ambient conditions for the test rig, which is suitable to investigate thermoacoustic transduction at relatively low frequencies using AM stacks for potential applications related to energy harvesting.

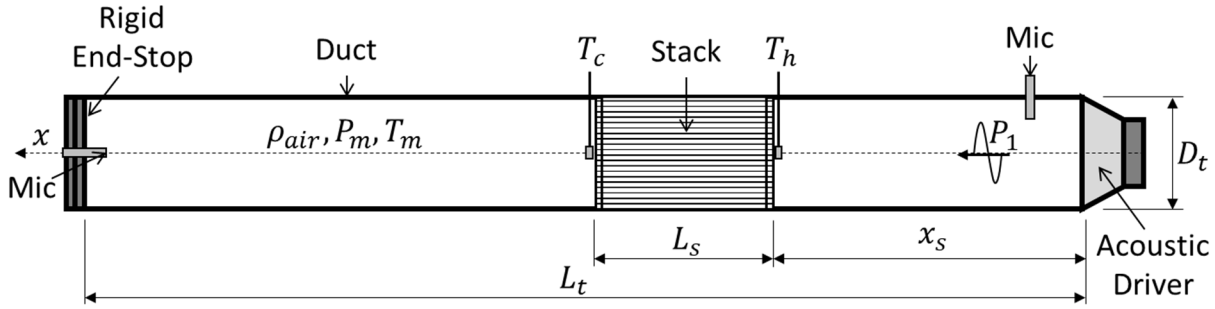

Figure 3. Schematic depiction of experimental parameters.

B. STACKS

The efficiency of a stack for a chosen working fluid is influenced by its pore geometry, while the optimum pore geometry is dependent on the thermal and viscous penetration depths [35] of the working fluid (air under ambient conditions). The thermal and viscous penetration depths for air are given by

$$\delta_k = \sqrt{\frac{2k}{\omega \rho c_p}} \tag{2}$$

$$\delta_v = \sqrt{\frac{2\mu}{\omega\rho}} \tag{3}$$

where k is thermal conductivity, $\omega = 2\pi f$ is the angular frequency, ρ is density, c_p is specific heat and μ is the dynamic viscosity of the working fluid. For given fluid property (Table 4) at room temperature and pressure, the thermal and viscous penetration depths at resonance frequency ($f_r = 113\ Hz$) are computed to be

$$\delta_k = 2.5 \times 10^{-4}\ m, \quad \delta_v = 2.14 \times 10^{-4}\ m \tag{4}$$

The geometric parameters of the stack are shown in Figure 4. The most important geometric parameters of the stack are the wall thickness ($2l$), pore width ($2y_0$), stack length (L_s) and porosity (ϕ) which is a function of pore width and wall thickness. To ensure an effective thermoacoustic cycle, the pore width ($2y_o$) should be on the order of two to four times the thermal and viscous penetration depths [40]. Therefore, for the current setup, the desired pore width ($2y_0$) ranges from 5.0×10^{-4} to 1.0×10^{-3} m. The geometrical properties of all the stacks studied are given in Table 1.

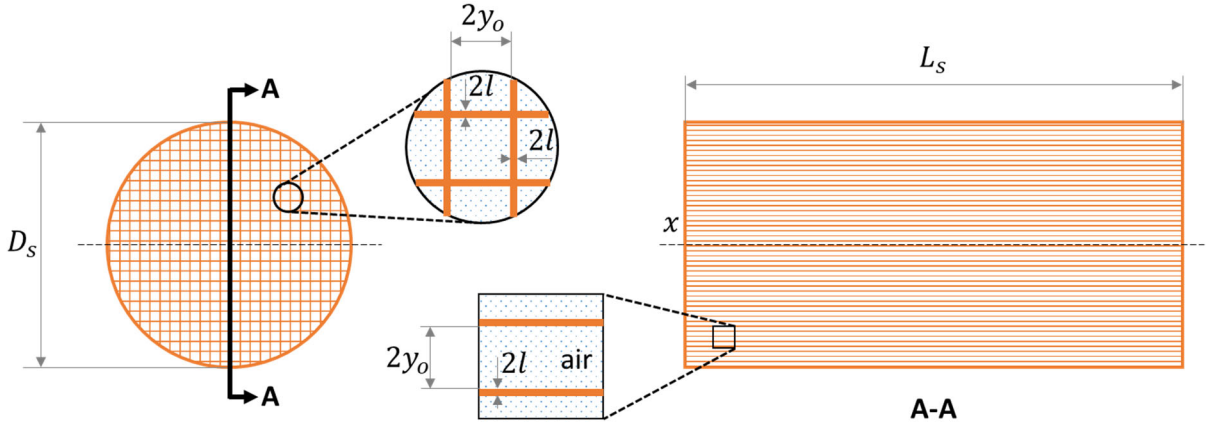

Figure 4. Diagram showing geometric parameters of a stack.

Table 1. Summary of ceramic and additively manufactured TAMS stack properties.

Property	CE170P80	CE178P85	PLA100P64	RES100P64	ASA100P64	PLA170P64	PLA100P44
Length, L_s, m	0.170	0.178	0.1	0.1	0.1	0.17	0.1
Diameter, D_s, m	0.097	0.0762	0.762	0.1	0.101	0.101	0.101
Areal porosity, ϕ	0.80	0.85	0.64	0.64	0.64	0.64	0.44
Pore wall thickness, $2l$, 10^{-4} m	1.01	1.01	5.0	5.0	5.0	5.0	5.0
Pore width, $2y_o$, 10^{-3} m	0.860	1.20	2.0	2.0	2.0	2.0	1.0
Material	Ceramic	Ceramic	PLA	Resin	ASA	PLA	PLA

The material properties of the stack also play a significant role in the performance of the thermoacoustic refrigerator and engine. In order to maintain a steady-state temperature gradient along with the stack plates, the stack material should have a higher heat capacity than the working fluid [35]. An optimal thermal conductivity also helps establish the requisite temperature gradient along the axial direction of the stack. A minimal pore wall thickness ($2l$) for the stack material enables creation of a higher areal porosity. Stacks with thicker pore walls also tend to create eddies at the corner, which contribute to a dissipative loss [36]. Various ceramic and additively manufactured (AM) stacks are considered in this study. Their details are summarized in Table 2. The ceramic stacks are sourced commercially from Corning's Celcor® line of filters and substrates, which are commonly used as conventional stacks for thermoacoustic devices [28]. These are manufactured through an extrusion process and can be obtained with different combinations of lengths, diameters, and pore geometry. For the present study,

two ceramic substrates of lengths around $0.17\ m$ and areal porosity of about 0.8 are chosen to act as the baseline stacks. For the AM stacks, commonly used polymeric materials and processes are considered. Three materials – Polylactic Acid (PLA), Formlabs® standard resin, and Acrylonitrile Styrene Acrylate (ASA) are considered. The material properties of the stacks are summarized in Table 2. The properties for the ceramic stack are estimated whereas those for the AM stacks are specified by the manufacturers.

Table 2. Mechanical and thermal properties of stacks.

Stack	Material	Thermal Conductivity (W/(m.K))	Specific Heat (J/(kg·K))	Melting Point (°C)	Density (kg/m^3)	Young's Modulus (GPa)	Poisson's Ratio
CE170P80	Ceramic	>1.5	352	>2000	2000-6000	>200	0.27
CE178P85	Ceramic	>1.5	352	>2000	2000-6000	>200	0.27
PLA100P6	PLA	0.13	1800	173	1240	3.5	0.3
PLA100P4	PLA	0.13	1800	173	1240	3.5	0.3
PLA170P64	PLA	0.13	1800	173	1240	3.5	0.3
ASA100P4	ASA	0.175	1300	135	1050	2.2	0.39
RES100P64	Resin	0.2	1000-1300	176	1250	2.7	0.35

PLA and ASA test stacks are fabricated using the Fused Deposition Modeling (FDM) process, and the resin test stack is fabricated using the stereolithographic (SLA) process. The lengths and porosity of the AM stacks are chosen as detailed in Table 2 to investigate the influence of these parameters. It is noted that while the AM processes chosen are affordable, they do also impose restrictions on the geometry and size of the pore structure that can be fabricated. All test stacks considered in this study have square pores. Photographs of the ceramic and AM stacks are shown in Figure 5.

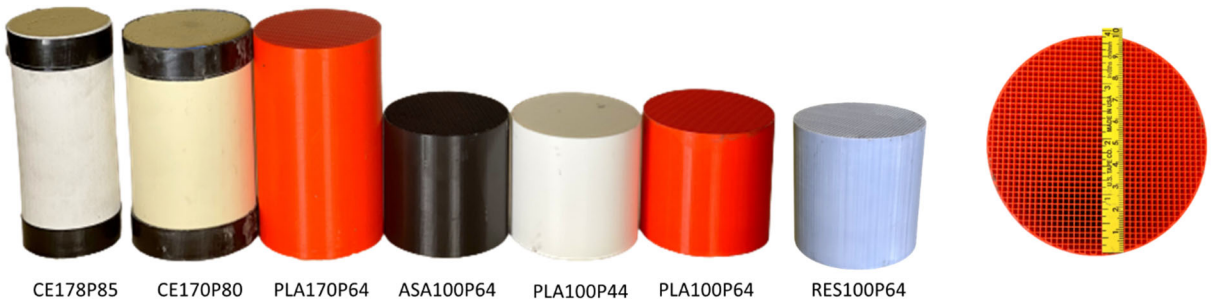

(a) (b)

Figure 5. (a) Photographs of various ceramic and AM stacks, (b) Porous structure of an AM stack.

C. THERMOELECTRIC GENERATOR (TEG)

Coupling the thermoacoustic refrigerator with a thermoelectric generator allows for harvesting of electrical energy from acoustic energy. We explore the feasibility of doing this using the Seebeck effect. While there are challenges to be addressed inasmuch as efficiency and power-to-volume ratio are concerned, this sequence of transduction for harvesting ambient acoustic energy offers advantages such as lack of moving parts or expendables [37]. As seen in Figure 6, the experiment is conducted in an anechoic chamber with thermal insulation around the TAMS resonator to reduce errors and improve efficiency. A thermopile consisting of 19 junctions of 24-gauge, nichrome-constantan wire junctions is arranged between the hot and cold sides of the stack as shown in Figure 6. Nichrome has a Seebeck coefficient (S_N) of 25 $\mu V/K$, whereas Constantan has a Seebeck coefficient (S_C) of -35 $\mu V/K$. The high contrast in their Seebeck coefficients makes them widely employed in thermoelectric applications. The theoretical voltage generated due to a temperature gradient, $\Delta T = T_h - T_c$ between the hot and cold side of the stack can be obtained as [38]

$$V = NS_{NC}\Delta T = N(S_N - S_C)(T_h - T_c) \tag{5}$$

where N is the number of thermocouple pairs in the thermopile.

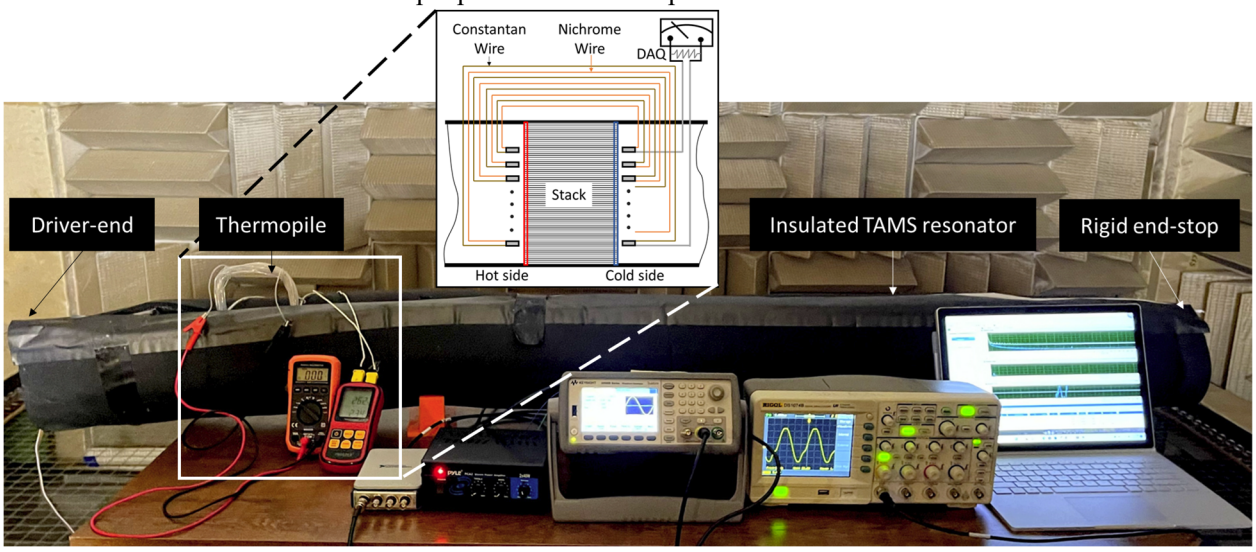

Figure 6. Photograph of the TAMS energy harvester with the thermoelectric circuit shown.

D. TEST CASES

The experimental test cases for the parametric study on different TAMS stacks are summarized in Table 3. Test cases are considered to evaluate the influence of parameters such as time to steady-state, acoustic excitation frequency, stack length, porosity, material, and position. For each case, the base parametric setting, $[P_m, T_m, P_1] = [1\ atm, 21\ ℃, 138\ dB]$ is preserved. Except for the stack position variation cases, all other cases have a stack position, $x_s = 0.1\ m$ (measured from the driver end). Multiple trials are considered for various cases, and in each case, the cold and hot side temperatures are recorded for discrete excitation frequencies spanning the frequency range of interest (80-140 Hz).

Table 3. Summary of experimental test cases.

Case #	Parameter	Values/ Type	Stacks	Measurements
t1-t4	Time to steady-state	$t \in [0,\ 45]\ min$	CE170P80, PLA170P64, PLA100P44, ASA100P64	T_c, T_h, P_1, t, f
f1-f7	Excitation frequency	$f \in [80,140]\ Hz$	All	T_c, T_h, P_1, f
L1, L2	Stack length	$L_s = [0.1,\ 0.17]\ m$	PLA100P64, PLA170P64	T_c, T_h, P_1, f
ϕ1, ϕ2	Stack porosity	$\phi = [0.64,\ 0.44]$	PLA100P64, PLA100P44	T_c, T_h, P_1, f
M1-M5	Stack material	Ceramic, PLA, ASA, Resin	CE170P80, PLA170P64 PLA100P64, ASA100P64, RES100P64	T_c, T_h, P_1, f
x1-x7	Stack position	$x_s = [0.1,\ 0.2,\ 0.3]\ m$	All	T_c, T_h, P_1, f_o

4. DISCUSSION OF RESULTS

A. PARAMETRIC STUDY

I. TIME TO STEADY-STATE

The time required to achieve a nearly steady state condition depends on various factors including the operating conditions and the geometrical configuration of the resonator. The evolution of the cold and hot-side temperatures for the ceramic stack CE170P80, at various acoustic excitation frequencies is shown in Figure 7. As the excitation frequency approaches closer to resonance, the difference in hot-side cold-side temperature becomes maximum. In general, the convergence to steady-state is found to be faster for the cold side compared to the hot side, although proximity of the excitation frequency to the resonance frequency does not seem to have any significant influence on the same. In all cases, nearly steady-state temperature gradient is established in about 20-25 minutes. Similar trends are seen for the additively manufactured stacks.

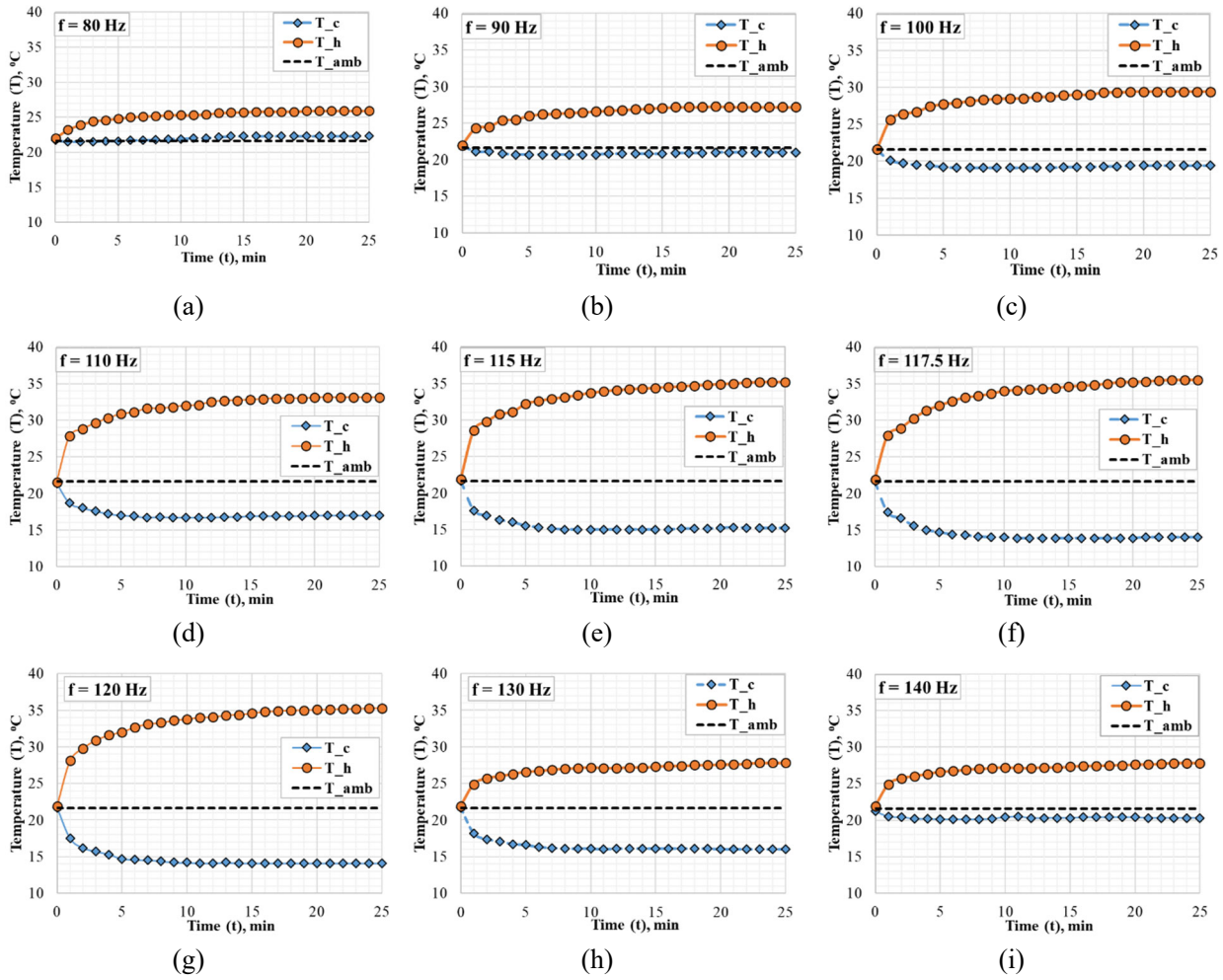

Figure 7. Evolution of cold and hot-side temperatures for the ceramic stack, CE170P80 for acoustic excitation frequencies of (a) 80, (b) 90, (c) 100, (d) 110, (e) 115, (f) 117.5, (g) 120, (h) 130 and (i) 140 Hz.

II. EXCITATION FREQUENCY

The steady-state temperature difference between hot and cold sides (ΔT) and the Carnot coefficient of performance for all stacks versus excitation frequency are shown in Figure 8. The stack position was retained at 0.1 m from the driver end for these cases. The temperature difference peaks in the frequency range of 110-120 Hz, with the peak value being obtained either at 115 or 117.5 Hz. This corresponds very well with the theoretically-computed resonance frequency for the thermoacoustic rig (113 Hz). In general, the AM stacks have comparable or better performance than the ceramic stacks considered. It is noted that both the ceramic stacks have higher porosity than the AM stacks but the diameter of the CE175P85 stack is markedly smaller than the

diameter of the resonator tube, which can explain its lower performance. Among the AM stacks, the resin and ASA stacks perform better than the PLA stacks.

Although the resin stack is not the longest nor does it have the best geometric parameters for its pores, the maximum temperature difference ($\Delta T = 24.8$ ℃) and the corresponding maximum Carnot efficiency (0.653) are obtained for the resin stack at an excitation frequency of 117.5 Hz. However, it was observed that its surface finish seems to be the best among all the stacks, potentially minimizing dissipative effects. Overall, AM stacks have the potential to deliver a similar or even better performance compared with conventional ceramic stacks while being more affordable, potentially lightweight, and amenable to more complex geometries, which could be useful to improve the power-to-volume ratio of thermoacoustic devices.

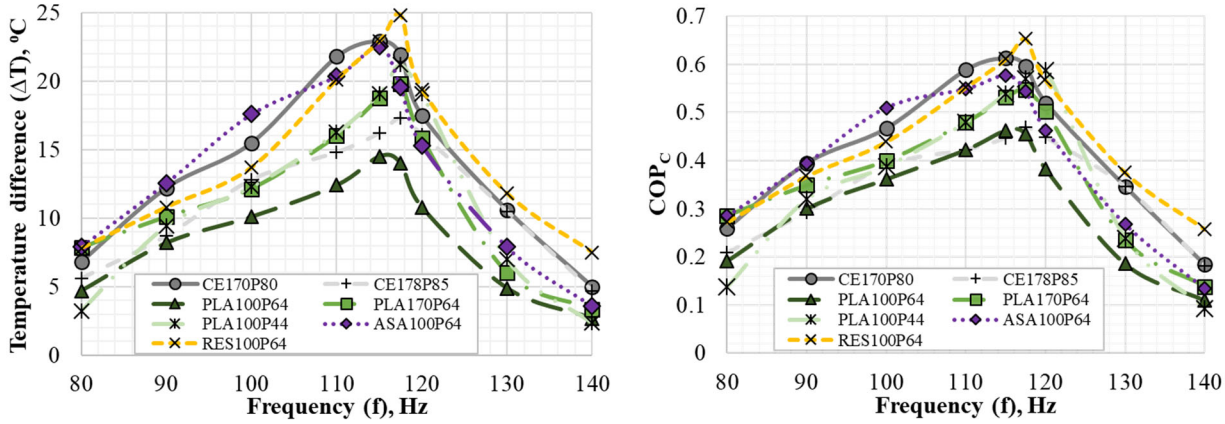

(a) (b)

Figure 8. Steady-state temperature difference between hot and cold sides and (b) coefficient of performance versus excitation frequency for ceramic and AM stacks. The stack position was set at $x_s = 0.1$ m.

III. STACK LENGTH

Stack length plays a very important role in the performance of a thermoacoustic device. The optimum length of the stack is influenced by the pressure and velocity of the gas parcel. The longer stack provides more surface area compared with the shorter stack which facilities more temperature drops across it. But at the same time, as the stack length increases more dissipative loss is experienced which affects the overall performance. In general, it is suggested to have a stack length of one-twentieth of the wavelength of the excitation [39]. The performance of two variants of PLA stack having different (0.1 m and 0.17 m) lengths with the same porosity are shown in Figure 9. The longer stack performs better over the entire frequency range of interest with an increase in a temperature difference of around 40% near resonance. A longer stack length tends to reduce the heat conducted through the stack walls between the hot and cold sides. When dissipative effects are small, this is seen to establish a higher temperature gradient between the hot and cold sides.

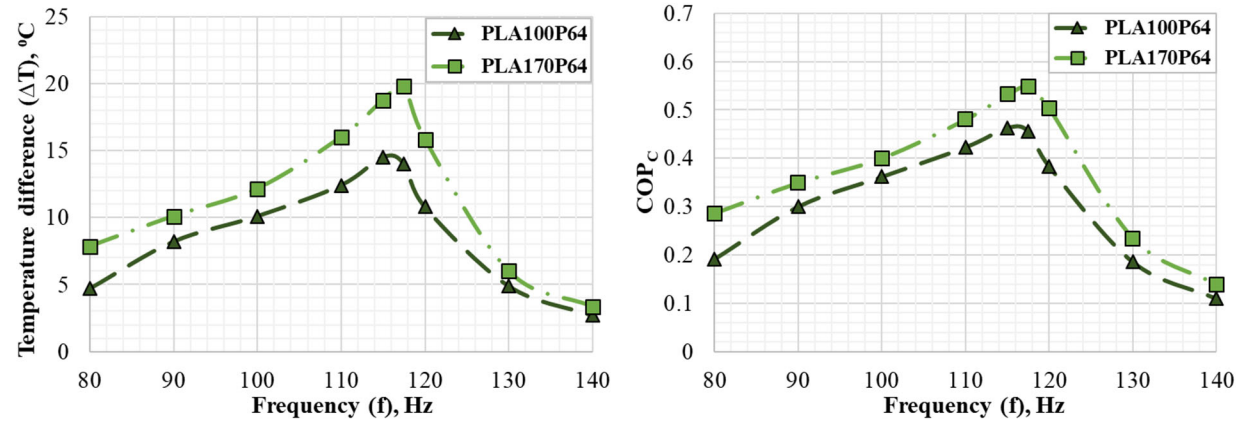

(a) (b)

Figure 9. (a) Steady-state temperature difference between hot and cold sides and (b) coefficient of performance versus frequency for PLA stacks of different lengths but same porosity. The stack position was set at $x_s = 0.1$ m.

IV. STACK POROSITY

The stack porosity is another important geometric parameter which directly contributes to the performance of a thermoacoustic device. With the decrease in porosity, more viscous losses occur when the gas parcel passes through the stack area. If the porosity is decreased drastically, the system will tend to lose its cooling function. In general, it is desirable to have a stack with higher porosity, as this implies more openings for the fluid to pass through the stack and thus it experiences less viscous losses on its way. The porosity of the stack can be increased either by increasing the pore width or by decreasing the wall thickness of the pore wall. In additive manufacturing, the minimum wall thickness that can be obtained is dependent on the material, process, and the specifications of the printer. Working with dimensions very close to the minimum thickness tends to result in poor tolerance and finish. Therefore, the wall thickness needs to be fixed at a feasible value and the pore width is changed to alter the porosity. However, the optimum pore width of the stack is stipulated by the thermal penetration depth of the fluid for a given temperature and pressure. At a resonance frequency of 117.5 Hz, the thermal penetration depth for air at room temperature is 2.42×10^{-4} m, so the optimum pore width in this case will be approximately 1×10^{-3} m.

Figure 10 shows a comparison of the performance of two PLA stacks that have different stack porosities. For this specific case, the stack with 44% porosity (PLA100P44) results in about a 50% increase in the temperature difference at resonance in comparison to the stack with 64% porosity (PLA100P64). Note that the lower porosity for PLA100P44 is realized by reducing the pore width but retaining the pore wall thickness the same as that for PLA100P64 as opposed to scaling both the width and wall thickness. Therefore, although the porosity is lower for the P44 stack, its pore width (1×10^{-3} m) is closer than that of the P64 stack (2×10^{-3} m) to four times the thermal penetration depth, which is recommended for optimal stack performance [40].

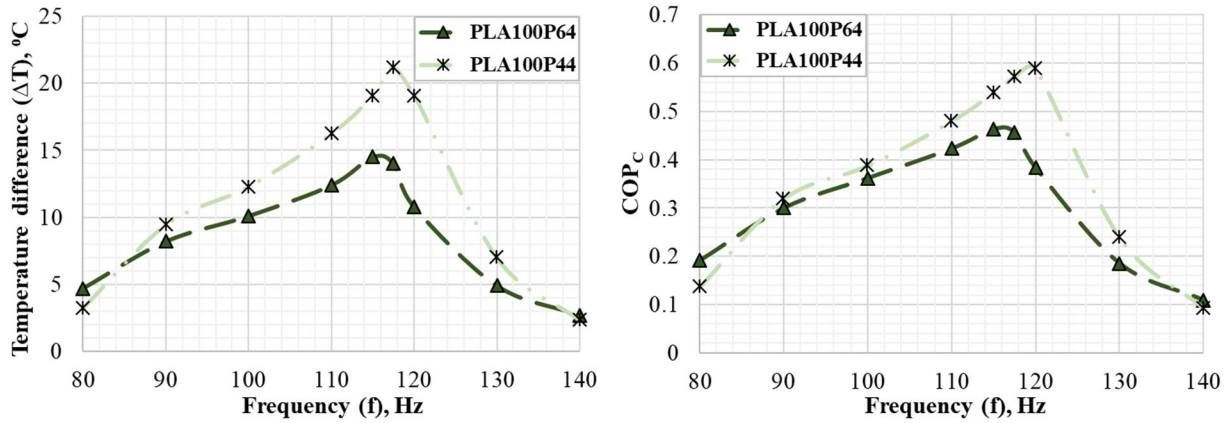

Figure 10. (a) Steady-state temperature difference between hot and cold sides and (b) coefficient of performance versus frequency for PLA stacks of different porosity but same lengths. The stack position was set at $x_s = 0.1$ m.

V. STACK MATERIAL

An important material property of the stack is its thermal conductivity. In general, it is desirable to have a stack with lower thermal conductivity as the effectiveness of the stack increases with decrease in thermal conductivity, as the heat conduction direction is opposite to the thermoacoustic heat transfer direction. Another important property of the stack is specific heat capacity. To extract useful work from acoustic waves via thermoacoustics, it is desirable to have a stack with higher specific heat capacity and a large surface area in contact with gas parcel so that the stack can exchange heat with the gas parcel without a significant temperature change of gas parcel. Figure 11 shows the comparison of the performance of three stacks fabricated with the same length and porosity using PLA, ASA, and resin. Among the AM stacks, the resin stack is found to perform the best. ASA stack has similar performance below resonance, but it drops below the resin stack at and above resonance. The performance of the PLA stack is markedly lower among the three. The best performance of the resin stack could be attributed, in part to its better surface finish among the AM stacks, while the PLA stack has a relatively poor surface finish which could increase dissipative losses. For the ceramic stacks, the porosity is higher due to the pore wall thicknesses being significantly lower than those for the AM stacks (Figure 12). Transitioning to AM processes that enable thinner pore wall thicknesses could result in improved performance for AM stacks.

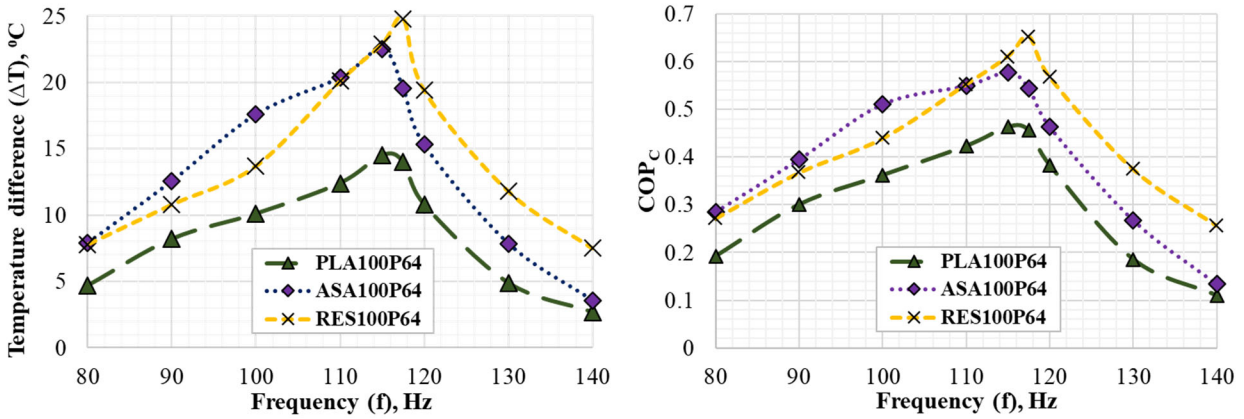

Figure 11. (a) Steady-state temperature difference between hot and cold sides and (b) coefficient of performance versus frequency for AM stacks of different material but same length and porosity. The stack position was set at $x_s = 0.1\ m$.

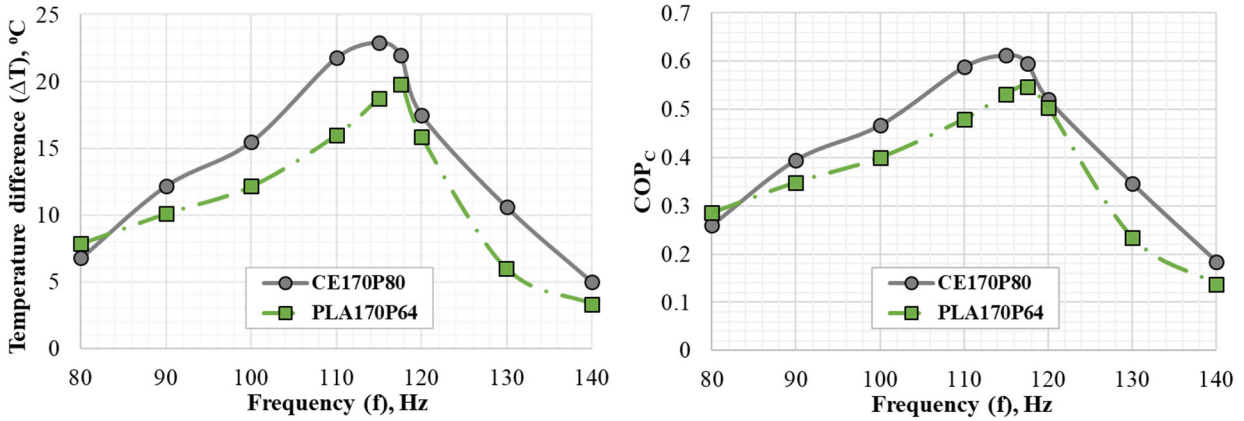

Figure 12. Comparison of (a) steady-state temperature difference between hot and cold sides and (b) coefficient of performance versus frequency for ceramic and PLA stacks of the same length. The stack position was set at $x_s = 0.1\ m$.

VI. STACK POSITION

The performance of a thermoacoustic device is influenced by the position of the stack inside the resonator tube. The optimum position of a stack inside the resonator tube depends on many factors, including the length of the stack. But in general, the stack performs its best when it is placed close to the pressure antinode. The temperature gradient obtained is proportional to the pressure amplitude difference between the ends of the stack.

Depending on the dimensions of the resonator tube, interactive effects are generated when the position of the stack is changed along the axis of the tube. For this closed-closed end configuration, pressure antinodes are located at both ends while velocity node is at the center. As shown in Figure 13, the location of the stack within the resonator tube is set at 0.1, 0.2, 0.3 and 0.48 m from the driver end. For each case, steady-state temperatures of both sides of the stack are recorded at resonance (117.5 Hz). In most cases, it is observed that the performance drops as the stack is moved more than 0.1 m away from the acoustic driver. The change of temperature gradient with stack position is seen to be lower for the ceramic stacks than those for AM stacks. While the resin stack had the best performance for a stack position $0.1\ m$ away from the acoustic driver, it drops considerably (nearly 50%) as the stack is moved farther away. Placing the stack extremely close to the driver could potentially trigger nonlinear effects which need to be investigated further.

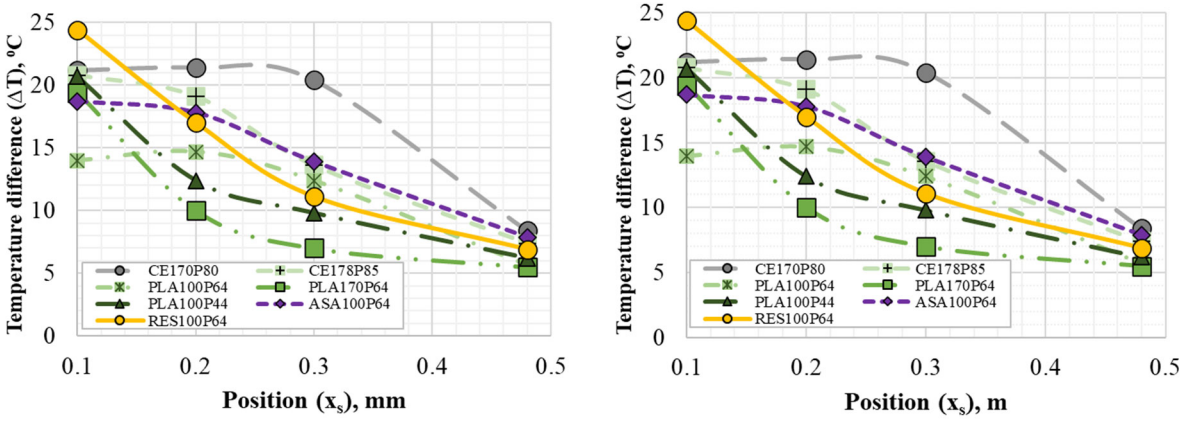

(a) (b)

***Figure 13**. (a) Steady-state temperature difference between hot and cold sides and (b) coefficient of performance versus stack position at an excitation frequency of 117.5 Hz (resonance) for ceramic and AM stacks.*

VII. ESTIMATION OF ERROR

Error bounds estimated from multiple trials for the evolution of the cold and hot-side temperatures to steady-state for the ceramic stack CE170P80, and the propagated error bounds for the steady-state temperature difference for ceramic and AM stacks are shown in Figure 14. The trials account for stack setup, data transduction, and initial condition-induced errors. Overall, the maximum error in the temperature measurement is within 1.5% for the ceramic stack, and the maximum error for the temperature difference for the ceramic and AM stacks is 15% near resonance (although errors for most data points are significantly smaller). The error bounds for the other cases are typically within these maximum values.

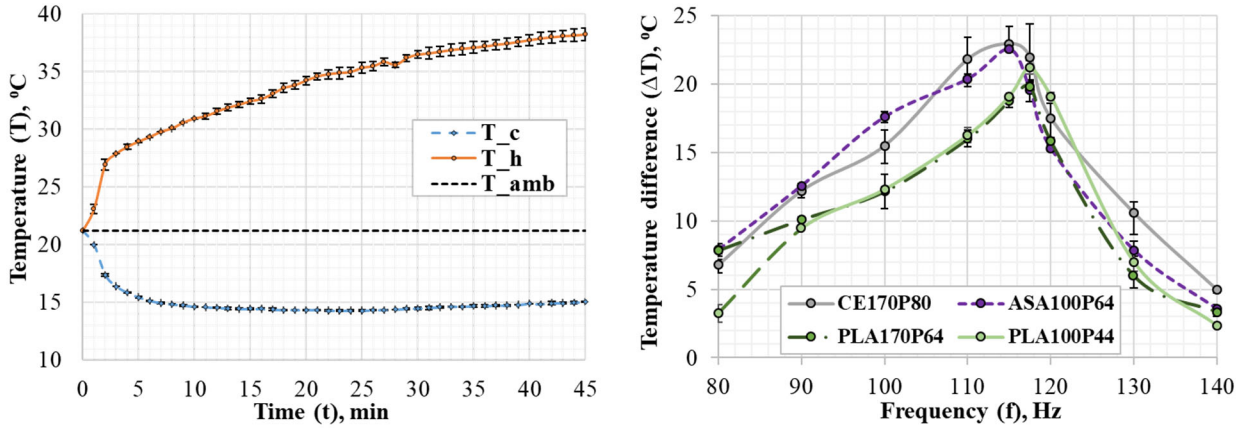

(a) (b)

Figure 14. Error bounds for (a) cold and hot-side temperatures versus time for the ceramic stack, CE170P80, and (b) steady-state temperature difference between hot and cold sides versus excitation frequency for ceramic and AM stacks. The stack position was set at $x_s = 0.1\ m$.

B. ENERGY HARVESTING

As seen from Figure 15(a), as the outputs evolve to steady-state a maximum voltage of 33 mV was generated for a temperature difference of 33.5 °C between the hot and cold sides of the stack at an acoustic excitation frequency of 117.5 Hz. Comparing the theoretical and experimental voltage outputs shown in Figure 15(b), it can be noted that though the reduction in the experimental output versus the theoretical prediction grows as the temperature gradient increases, an efficiency of about 85% is still obtained at maximum output.

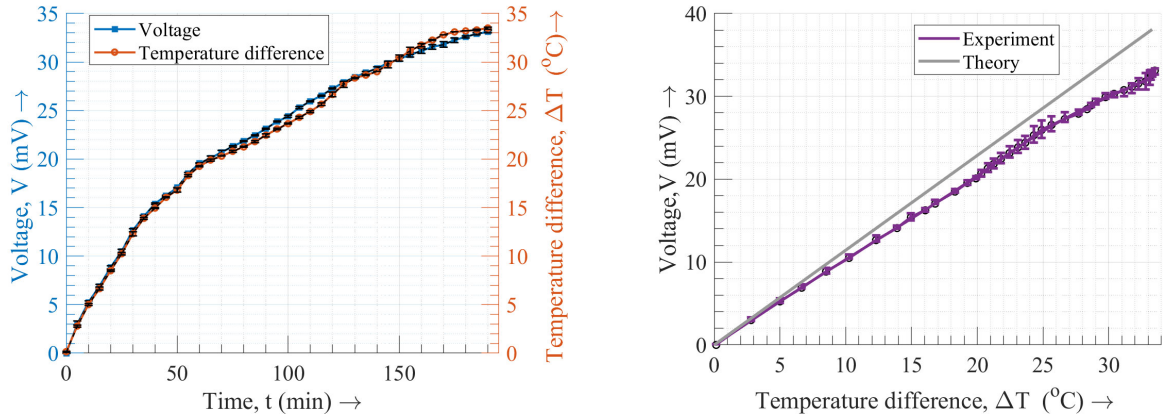

Figure 15. Energy harvesting output from TAMS: (a) Voltage and temperature time histories, and (b) Comparison of theoretical and experimental voltage output.

C. SOUND TRANSMISSION LOSS

It is of interest to investigate the sound transmission loss across the TAMS stack in order to gauge the contribution of the thermoacoustic conversion to the reduction in sound pressure level. For this purpose, one microphone was placed at the driver end and one at the closed end to extract the standing wave pressure time histories while thermoacoustic steady-state was established. The incident and transmitted-side microphone signals from preliminary results are shown in Figure 16. Preliminary results show a reduction in SPL of around 5.28 dB between the far end and driver end at resonance (117.5 Hz). This reduction of noise level is due to the placement of a stack in the sound path between the sound source and the closed end which could also be termed an insertion loss.

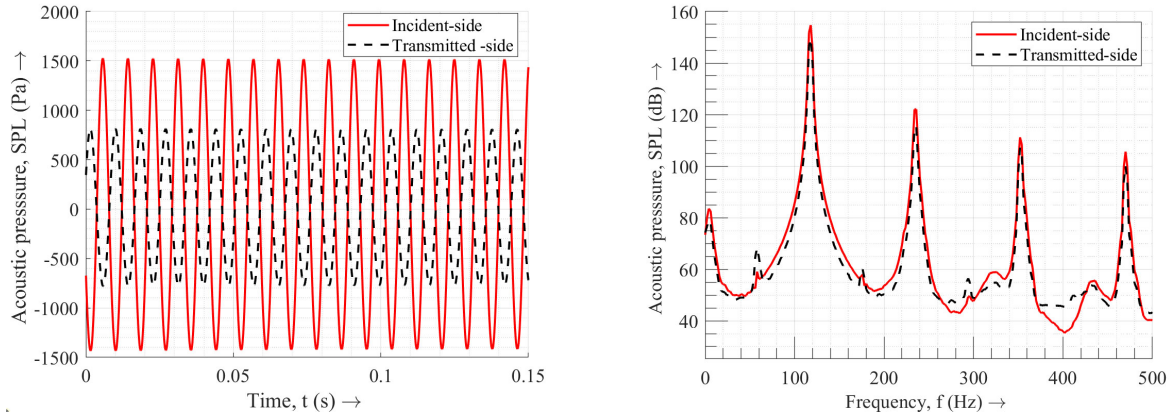

Figure 16. (a) Acoustic pressure vs. time plot of driver end and far end, (b) Acoustic pressure level vs. frequency plot of driver end and far end.

D. DELTAEC SIMULATION

The performance of the thermoacoustic devices based on Rott's linear approximation [5] can be predicted using the open-source software, Design Environment for Low-amplitude Thermoacoustic Energy Conversion (DeltaEC) [19]. DeltaEC computes the resonance frequency for a given geometry of the stack and waveguide and the properties of the working fluid. Steady-state temperature gradient between the hot and cold-sides of the stack can also be computed for different excitation frequencies and geometric and material configurations. . DeltaEC has different segments for each element of geometry. Wave propagation within each segment relies on local parameters such as area and perimeter and global parameters such as frequency [19].

The magnitude and phase of acoustic pressure (P_1) and the magnitude and phase of the volumetric flow rate (U_1) were defined as the four-initial condition. Infinite acoustic impedance boundary conditions were imposed at the end of the final segment. In this case, the solid wall of the duct segment has been assumed to be laterally

ideal to impose a perfect isothermal boundary condition. Air at room temperature and atmospheric pressure is used as the working fluid. Its properties are given in Table 4. The exact geometrical and thermophysical properties of the fabricated stack can differ from the designed parameters and bulk material properties. Where possible, measured values are used for the resin stack in the DeltaEC simulations (Table 5).

Table 4. Properties of air at atmospheric pressure and temperature

Property	**Value**	**Source/ Ref**
Thermal conductivity (k), W/(m.K)	0.025	[19]
Sound velocity (a), m/s	343	[19]
Specific heat ratio of air (γ)	1.4	[19]
Heat capacity (C_p), J/(kg. K)	1004.7	[19]
Dynamic viscosity (μ), kg/(s.m)	1.817×10^{-5}	[19]
Prandtl number (σ)	0.70	[19]
Air density (ρ), kg/m^3	1.118	[19]
Gas constant (R), kJ/(kg.K)	0.287	[19]
Thermal diffusivity (κ), m^2/s	2.17×10^{-5}	[19]

Table 5. Measured geometric parameters and thermophysical properties of the resin stack (RES100P64)

Geometric parameter/ Thermophysical property	**Value**	**Source/ Ref**
Length (L_s), m	0.1	Measured
Diameter (D_s), m	0.1	Measured
Areal porosity (ϕ)	0.39	Measured
Average pore wall thickness $(2l)$, m	7.9×10^{-4}	Measured
Average pore width $(2y_o)$, m	1.59×10^{-3}	Measured
Thermal Conductivity (k), W/(m.K)	0.31	[41]
Heat capacity (c), J/(kg.K)	1466	[42]
Density (ρ), kg/m^3	1081	[42]

As shown in Figure 17(a), preliminary simulations captured the trend and peak frequency with good accuracy. Nominal thermophysical parameters were used for the simulation. The use of measured thermophysical properties could provide better correlation of DeltaEC predictions with the experimental result. Figure 17(b) shows the simulated and experimental temperature gradients achieved for different stack positions inside the resonator tube. The maximum temperature gradient is observed for the stack position between 0.05 m to 0.250 m from the driver end. The temperature gradient drops as the stack is moved from the driver end to the center of the resonator tube. The minimum temperature gradient is observed at the center of the resonator tube where the acoustic pressure is minimum. The temperature gradient starts increasing as stack is moved to the closed end due to the increase in acoustic pressure.

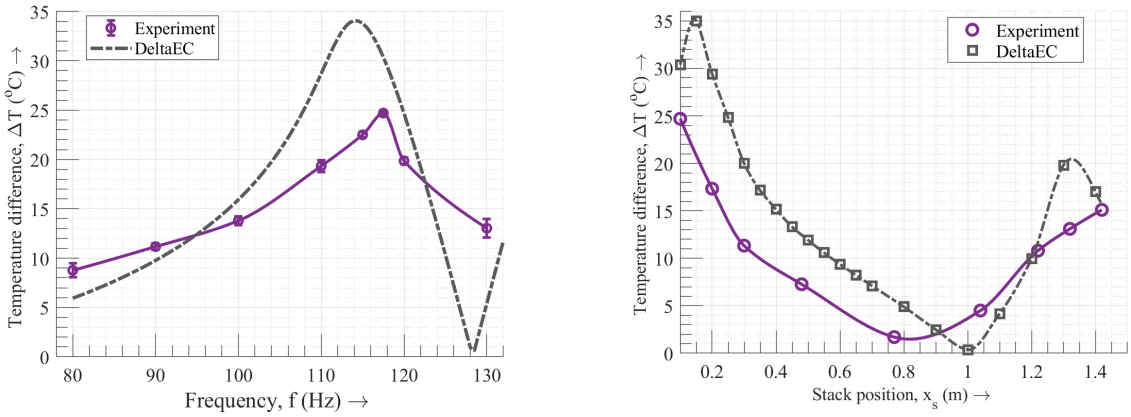

(a) (b)

Figure 17. Comparison of experimental and simulated parameters for RES100P64: Temperature gradient versus (a) excitation frequency and (b) stack position.

4. CONCLUSION

A mechanically robust, noise mitigating, energy harvesting metastructure is explored using thermoacoustic and thermoelectric transduction approaches. Drawing inspiration from acoustic metamaterials, such a thermoacoustic metastructure (TAMS) is designed to consist of an additively manufactured porous stack housed within an acoustic resonator and equipped with a thermopile for energy harvesting. Firstly, an experimental parametric study was conducted to evaluate various additively manufactured stack designs against more conventional ceramic stacks using a benchtop thermoacoustic rig. The influence of parameters such as time to steady-state, excitation frequency, stack material, length, porosity, and position on the performance are examined. It is found that the hot and cold-side temperatures evolve to steady-state under 25 minutes, with the rate of convergences being faster for the cold-side as well as for the ceramic stacks. The temperature gradient and efficiency are found to peak between acoustic excitation frequencies of 115 and 120 Hz. Among all cases, the resin stack showed the largest temperature gradient of about 24.8 ℃ at 117.5 Hz. Stack positions close to the source are found to be more efficient. In general, the performance of AM stacks is found to be comparable to ceramic stacks, although several of the parameters involved could be further optimized. Preliminary results also show a reduction in SPL of around 5.28 dB between the far end and driver end at resonance (117.5 Hz). Next, an acousto-thermo-electric transduction scheme is employed to harvest usable electrical power using the best performing stack. The temperature gradient and efficiency are found to peak for an excitation at 104 dB with a frequency of about 117.5 Hz. The resin stack showed the largest temperature gradient of about 33.5 ℃ at 117.5 Hz. A peak voltage of 33 mV at an output power of 19.8 μW was generated for this temperature gradient using a 19-junctions thermopile based on the Seebeck effect. Optimization of the energy harvesting process is being investigated to improve power generation. Preliminary results also show potential for noise mitigation in conjunction with energy harvesting. With current additive and hybrid fabrication processes and materials reaching commercial maturity, opportunities exist to employ such TAMS embedded within modular infrastructural building-blocks that could be arrayed as a multifunctional barrier separating a noise-rich environment from zones that could benefit from acoustic shielding.

ACKNOWLEDGEMENTS

Support from NSF RII Track-4 Grant No. 2033399 is gratefully acknowledged. Thanks are due to graduate student Oluwafemi Akinmolayan, for help with the experiments.

REFERENCES

1. Rijke, P. L. Notiz Über Eine Neue Art, Die in Einer an Beiden Enden Offenen Röhre Enthaltene Luft in Schwingungen Zu Versetzen. *Annalen der Physik und Chemie*, **183 (6),** 339–3431 (1859).
2. Heidelberg, N. Zu. Verhandlungen Des Naturhistorisch-Medizinischen Vereins Zu Heidelberg. *Naturhistorisch-Medizinischen Vereins zu Heidelber, Naturhistor.-Med. Verein*, (1965).

3. Kirchhoff, G. On the Influence of Heat Conduction in a Gas on Sound Propagation. *Annual Review of Physical Chemistry*, **134**, 177–193, (1868).
4. Rott, N. Thermoacoustics. *Advances in Applied Mechanics*, **20**, 135–175, (1980).
5. Rott, N. Damped and Thermally Driven Acoustic Oscillations in Wide and Narrow Tubes. *Zeitschrift für Angewandte Mathematik und Physik ZAMP*, **20 (2)**, 230–243, (1969).
6. Rott, N. & Zouzoulas, G. Thermally Driven Acoustic Oscillations, Part IV: Tubes with Variable Cross-Section. *Journal of Applied Mathematics and Physics*, **27 (2)**, 197–224, (1976).
7. Swift, G. W. Analysis and Performance of a Large Thermoacoustic Engine. *The Journal of the Acoustical Society of America*, **92 (3)**, 1551–1563, (1992).
8. Backhaus, S. & Swift, G. W. A Thermoacoustic-Stirling Heat Engine: Detailed Study." *The Journal of the Acoustical Society of America*, **107**, 1145, (2000).
9. Gardner, D.L. & Swift, G.W. A Cascade Thermoacoustic Engine. *Journal of Acoustic Society of America,* **114**, 1905–1919, (2003).
10. Tijani, M. Loudspeaker-Driven Thermo-Acoustic Refrigeration. *Phd Thesis, Technische Universiteit Eindhoven,* (2001).
11. Paek, I., Braun, J.E. & Mongeau, L. Evaluation of Standing-Wave Thermoacoustic Cycles for Cooling Applications. *International Journal of Refrigeration*, **30**, 1059–1071 (2007).
12. Raut, A.S. & Wankhede, U.S. Review of Investigations in Eco-Friendly Thermoacoustic Refrigeration System. *Thermal Science*, **21**, 1335–1347, (2017).
13. Yahya, S.G., Mao, X. & Jaworski, A.J. Experimental Investigation of Thermal Performance of Random Stack Materials for use in Standing Wave Thermoacoustic Refrigerators. *International Journal of Refrigeration*, **75**, 52–63, (2017).
14. Jin, T., Huang, J., Feng, Y., Yang, R., Tang, K., & Radebaugh, R. Thermoacoustic Prime Movers and Refrigerators: Thermally Powered Engines Without Moving Components. *Energy*, **93**, 828–853, (2015).
15. Setiawan, I., Achmadin, W. N., Murti, P. & Nohtomi, M. Experimental Study on a Standing Wave Thermoacoustic Prime Mover with Air Working Gas at Various Pressures. *Journal of Physics: Conference Series*, **710 (1)**, (2016).
16. Hamood, A., Jaworski, A. J. & Mao, X. Development and Assessment of Two-Stage Thermoacoustic Electricity Generator. *Energies*, **12 (9)**, 1-18, (2019).
17. Swift, G.W. Thermoacoustics. *Acoustical Society of America,* (2017).
18. Alcock, A. C., Tartibu, L. K., & Jen, T. C. Design and Construction of a Thermoacoustically Driven Thermoacoustic Refrigerator. *Proceedings of the Conference on the Industrial and Commercial Use of Energy, ICUE*, 1–7, (2017).
19. Clark, J. P., Ward, W. C. & Swift, G. W. Design Environment for Low-Amplitude Thermoacoustic Energy Conversion (DeltaEC). *The Journal of the Acoustical Society of America*, **122 (5)**, 3014, (2010).
20. Timmer, M.A., de Blok, K. & van der Meer, T.H. Review on the Conversion of Thermoacoustic Power into Electricity. *The Journal of the Acoustical Society of America,* **143 (2)**, 841-857, (2018).
21. Yuan, M., Cao, Z., Luo, J. & Chou, X. Recent Developments of Acoustic Energy Harvesting: A Review. *Micromachines*, **10 (1)**, 48, (2019).
22. Zhao, D. Waste Thermal Energy Harvesting from a Convection-Driven Rijke–Zhao Thermo-acoustic-piezo System. *Energy Conversion and Management*, **66**, 87-97, (2013).
23. Nouh, M., Aldraihem, O. & Baz, A. Transient Characteristics and Stability Analysis of Standing Wave Thermoacoustic-Piezoelectric Harvesters. *The Journal of the Acoustical Society of America*, **135 (2)**, 669-678, (2014).
24. Avent, A.W. & Bowen, C.R. Principles of Thermoacoustic Energy Harvesting. *The European Physical Journal Special Topics*, **224 (14)**, 2967-2992, (2015).
25. Jensen, C. & Raspet, R. Thermoacoustic Power Conversion Using a Piezoelectric Transducer. *The Journal of the Acoustical Society of America*, **128 (1)**, 98-103, (2010).
26. Thomann, H. Piezoelectric Ceramics. *Advanced Materials*, **2 (10)**, 458-463, (1990).
27. Noh, S., Lee, H. & Choi, B. A Study on the Acoustic Energy Harvesting with Helmholtz Resonator and Piezoelectric Cantilevers. *International Journal of Precision Engineering and Manufacturing*, **14 (9)**, 1629-1635, (2013).
28. Khan, F.U. Electromagnetic Energy Harvester for Harvesting Acoustic Energy. *Sādhanā*, **41 (4)**, 397-405, (2016).
29. Khan, F. & Izhar. Piezoelectric Type Acoustic Energy Harvester with a Tapered Helmholtz Cavity for Improved Performance. *Journal of Renewable and Sustainable Energy*, **8 (5)**, 054701, (2016).
30. Ceperley, P.H. A Pistonless Stirling Engine—The Traveling Wave Heat Engine. *The Journal of the Acoustical Society of America*, **66 (5)**, 1508-1513, (1979).
31. Tward, E., Petach, M. & Backhaus, S.Thermoacoustic Space Power Converter. *AIP Conference Proceedings***, 654 (1)**, 656-661, (2003).
32. Garrett, S.L., Adeff, J.A. Hofler, T.J. Thermoacoustic Refrigerator for Space Applications. *Journal of Thermophysics and Heat Transfer*, **7 (4)**, 595-599, (1993).
33. Yu, Z., Jaworski, A.J. & Backhaus, S. A Low-cost Electricity Generator for Rural Areas Using a Travelling-wave Looped-tube Thermoacoustic Engine. *Proceedings of the Institution of Mechanical Engineers, Part A: Journal of Power and Energy*, **224 (6)**, 787-795, (2010).

34. Chen, B.M., Riley, P.H., Abakr, Y.A., Pullen, K., Hann, D.B. & Johnson, C.M. Design and Development of a Low-cost, Electricity-generating Cooking Score-Stove™. *Proceedings of the Institution of Mechanical Engineers, Part A: Journal of Power and Energy*, **227 (7)**, 803-813, (2013).
35. Tijani, M.E.H., Zeegers, J.C.H. & De Waele, A.T.A.M. Design of Thermoacoustic Refrigerators. *Cryogenics*, **42**, 49–57 (2002).
36. Tasnim, S.H. Porous Media Thermoacoustic Stacks: Measurements and Models. *Ph.D. Thesis, University of Waterloo* (2011).
37. Enescu, D. Thermoelectric Energy Harvesting: Basic Principles and Applications. *Green Energy Advances*, **1**, (2019).
38. Yang, M.Z., Wu, C.C., Dai, C.L. & Tsai, W.J. Energy Harvesting Thermoelectric Generators Manufactured Using the Complementary Metal Oxide Semiconductor Process. *Sensors*, **13 (2)**, 2359-2367, (2013).
39. Wetzel, M., & Herman, C. Design Optimization of Thermoacoustic Refrigerators. *International Journal of Refrigeration*, **20 (1)**, 3-21, (1997).
40. Wheatley, J., Hofler, T., Swift, G.W. & Migliori, A. Understanding Some Simple Phenomena in Thermoacoustics with Applications to Acoustical Heat Engines. *American Journal of Physics,* **53 (2)**, 147-162, (1985).
41. Kelava, L., Ivić, I., Pakai, E., Fekete, K., Maroti, P., Told, R., Ujfalusi, Z. & Garami, A. Stereolithography 3D Printing of a Heat Exchanger for Advanced Temperature Control in Wire Myography. *Polymers*, **14 (3)**, 471, (2022).
42. Brooks, H., Wright, C., Harris, S. & Fsadni, A. Fire Resistance of Additively Manufactured Water Filled Polymer Parts. *Additive Manufacturing*, **22**, 138-145, (2018).